Enhanced magnetic moments in Mn-doped FeCo clusters owing to ferromagnetic surface Mn atoms

Masahiro Sakurai[1,*] and James R. Chelikowsky[1,2,3]
[1]*Center for Computational Materials, Oden Institute for Computational Engineering and Sciences, The University of Texas at Austin, Austin, Texas 78712, USA*
[2]*Department of Chemical Engineering, The University of Texas at Austin, Austin, Texas 78712, USA*
[3]*Department of Physics, The University of Texas at Austin, Austin, Texas 78712, USA*

(Received 7 January 2019; published 8 April 2019)

We provide an avenue to achieve optimized magnetic properties without relying on rare-earth elements. In particular, we focus on transition-metal nanoparticles with magnetic ordering that is rarely seen in bulk. By using first-principles real-space pseudopotential calculations, we show that Mn can exhibit ferromagnetic behavior similar to Fe when Mn is placed on the surface of a FeCo cluster. This ferromagnetic behavior of surface Mn is in sharp contrast with Mn bulk and Mn-based alloys, which are either antiferromagnetic or paramagnetic. The local magnetic moment carried by a surface Mn atom is larger than those of Fe and Co, leading to an increase of the total magnetic moment. We find that surface-Mn-induced magnetic enhancement is robust in ternary MnFeCo clusters with different sizes and various chemical compositions. Our theoretical findings provide a useful guide for designing new nanoparticles with a large magnetic moment.

DOI: 10.1103/PhysRevMaterials.3.044402

I. INTRODUCTION

Magnetism of transition-metal nanoclusters [1] often deviates significantly from bulk owing to the reduced coordination number of surface atoms and possible lattice relaxations or reconstructions at a cluster surface. For example, Rh is paramagnetic in the bulk phase, while Rh nanoclusters are found to be ferromagnetic [2]. Distinct magnetic properties exhibited on a nanoscale offer great potential for applications such as magnetic storage and spintronic devices [3]. It is highly desirable to achieve such novel, potentially useful magnetic properties without using rare-earth elements. Concerns about a reliable supply of rare-earth elements have continued to grow in recent years [4,5].

Binary Fe-Co alloys and nanoclusters are interesting magnetic materials among transition-metal-based materials, particularly because of their high magnetization. Doping of additional elements may control the magnetic properties of a parent compound, making it possible to optimize the performance as a strong magnet. For example, ferrite compounds, which have been commonly used in applications, are made by mixing iron oxides with additional metallic elements, such as Mn, Ni, Zn, and Ba. Here, we focus on the role of Mn in the Fe-Co system owing to the recent synthesis of Mn-Fe-Co ternary systems [6]. The abundance of Mn in the upper continental crust of the Earth [4] is an obvious advantage over the relatively scarce rare-earth elements, such as Sm and Dy.

Magnetic ordering in Mn bulk [7,8] and Mn-based alloys [9–11] is antiferromagnetic or paramagnetic. In particular, the total magnetic moment in Mn-Fe alloys [9,10] and Mn-Co alloys [11] decreases linearly with increasing Mn concentration. This is because the local magnetic moment from Mn couples to neighboring moments in an antiferromagnetic manner, canceling out each other. The magnetizations of the above Mn-based alloys obey the Slater–Pauling magnetization curve [12,13] that gives magnetization as a function of the number of the valence electrons per atom for transition-metal alloys.

Stern–Gerlach experiments on Mn-doped transition-metal clusters [14], followed by theoretical work on small binary transition-metal clusters [15–17], have shown possible ferromagnetic behavior of Mn-doped clusters and deviation from the Slater–Pauling rule. Ferromagnetism along with high magnetization well above the Slater–Pauling curve has also been reported recently in Mn-Fe-Co ternary thin films [6,18] and in Mn-Si nanoparticles [19]. In particular, it was found that the total magnetic moment can increase with Mn concentration in MnCo clusters, which is in sharp contrast with MnCo alloys. The overall trend of the observed ferromagnetic behavior of MnCo clusters [14] has been interpreted by the virtual bound-state (VBS) model [20]. However, the intrinsic mechanism behind the ferromagnetic behavior of Mn-doped nanoclusters and their enhanced total magnetic moments remain unclear.

First-principles calculations are a powerful approach to study magnetic phenomena. Specifically, a real-space pseudopotential formalism [21–23] coupled with the density-functional theory (DFT) [24,25] works well to describe ferromagnetism as well as noncollinear magnetism in elemental transition-metal nanoclusters [26–29]. Theoretical investigations using first-principles calculations are helpful to clarify a detailed picture of the magnetic properties of Mn-doped alloy clusters.

In this paper, we employ first-principles real-space pseudopotential calculations to study Mn-doped FeCo clusters, with emphasis on the influence of Mn dopants on the structural and magnetic properties of MnFeCo ternary alloy clusters. We show that Mn prefers surface sites for substitution.

*masahiro@ices.utexas.edu

Surface Mn couples to neighboring Fe and Co atoms in a ferromagnetic manner and carries a larger local moment than Fe and Co, leading to an increase of the total magnetic moment. Magnetic enhancement is expected in MnFeCo clusters with various sizes and different compositions.

II. COMPUTATIONAL METHODS

We perform first-principles calculations in the framework of DFT [24,25] combined with a real-space pseudopotential method as implemented in the PARSEC code [21–23]. We adopt the generalized gradient approximation (GGA) for the exchange-correlation functional [30]. Nanoparticles with different magnetic orderings are studied by solving the generalized 2×2 Kohn–Sham equations [29,31], which include the noncollinear spin density, $\vec{m}(\vec{r})$. The Kohn–Sham equation is solved self-consistently on a uniform grid in real space. The Laplacian operator in the kinetic-energy term is expanded by a high-order finite-differencing scheme with a grid spacing of 0.3 a.u. (approximately 0.16 Å), which is fine enough to give the total energy with a convergence of less than 1 meV/atom for $3d$ transition-metal clusters [27,28,32]. A spherical domain is used as a boundary condition to simulate an isolated cluster. The wave functions are sampled inside the domain and vanish beyond the domain boundary (10 a.u. away from the outermost atom of a cluster). We employ norm-conserving pseudopotentials [33] that include a partial core correction [34]. Pseudopotentials are constructed with s, p, d core radii (in a.u.) of 2.32, 2.57, 2.32 for Mn, 2.18, 2.38, 2.18 for Fe, and 2.18, 2.38, 2.18 for Co. Structural relaxations [35–37] are performed until a residual force is less than 0.01 Ry/a.u. In the PARSEC code, several numerical algorithms play vital roles to reduce computational costs. In particular, iterations to obtain a self-consistent solution to the Kohn–Sham equation are done by a subspace filtering technique with Chebyshev polynomials [38–40]. Our filtering algorithms avoid any full diagonalizations and can reduce computational time by more than an order of magnitude in comparison with conventional diagonalization-based methods.

III. RESULTS

A. Case study of 28-atom clusters

We examine the magnetic coupling of substituted Mn to neighboring Fe and Co by taking a $MnFe_{13}Co_{14}$ cluster (Fig. 1) as an example. Fe and Co atoms are initially arranged in a body-centered cubic (bcc) coordination, forming a truncated B2-ordered cluster. One of the Fe atoms are substituted with a Mn atom and atomic positions are then optimized. We performed not only spin-polarized calculations, which assume collinear magnetism, but also noncollinear magnetic calculations to take into account spin orientations explicitly. The calculated total energy and the total magnetic moment of a $MnFe_{13}Co_{14}$ cluster are listed in Table I. We find that the total energy is lower when all spins are ordered in a ferromagnetic manner. This ferromagnetic behavior of Mn is in sharp contrast to Mn bulk [7,8] and Mn-based alloys [9–11], which are either antiferromagnetic or paramagnetic. As the system prefers ferromagnetic ordering, results from spin-polarized calculations are consistent with those from noncollinear magnetic calculations with all spins oriented to the z axis. This indicates that the spin-polarized (collinear) formalism works well to describe the ferromagnetism in a ternary MnFeCo cluster.

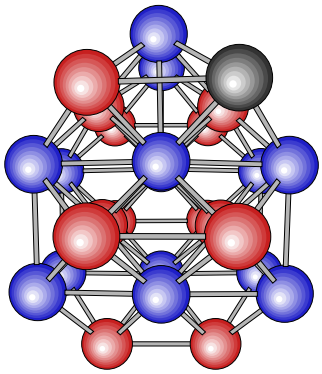

FIG. 1. Ball-and-stick model of a $MnFe_{13}Co_{14}$ cluster with a body-centered cubic coordination where Fe and Co atoms are arranged in the B2-type structure. Gray, red, and blue spheres represent Mn, Fe, and Co atoms, respectively.

We focus on $MnFe_{14}Co_{13}$ and $MnFe_{13}Co_{14}$ clusters to determine the energetically preferable site for Mn substitution and its impact on the total magnetic moment. Figure 2 shows the binding energies and total magnetic moments calculated for $MnFe_{14}Co_{13}$ and $MnFe_{13}Co_{14}$ clusters. We find that surface sites are preferable for Mn substitution. This agrees generally with previous calculations on small binary clusters of Mn-Fe and Mn-Co [15,16]. Fe is more likely to be substituted than Co because the binding energy of a $MnFe_{13}Co_{14}$ cluster is larger than that of a $MnFe_{14}Co_{13}$ cluster. As shown in Fig. 2(b), clusters with surface Mn have a larger total magnetic moment, whereas interior Mn does not increase the total magnetic moment.

TABLE I. Total energy and total magnetic moment of a $MnFe_{13}Co_{14}$ cluster obtained by spin-polarized and noncollinear magnetic calculations. The total energy is measured relative to the spin-polarized ("collinear") calculation.

	Orientation of local magnetic moments		Total energy	Total magnetic moment
Method	Fe and Co sites	Mn site	E (meV/atom)	M (μ_B/cluster)
GGA with spin polarization	"collinear"	"collinear"	0	68.3
GGA with noncollinear magnetism	parallel to z axis	parallel to z axis	0	68.3
GGA with noncollinear magnetism	parallel to z axis	antiparallel to z axis	+14	59.3

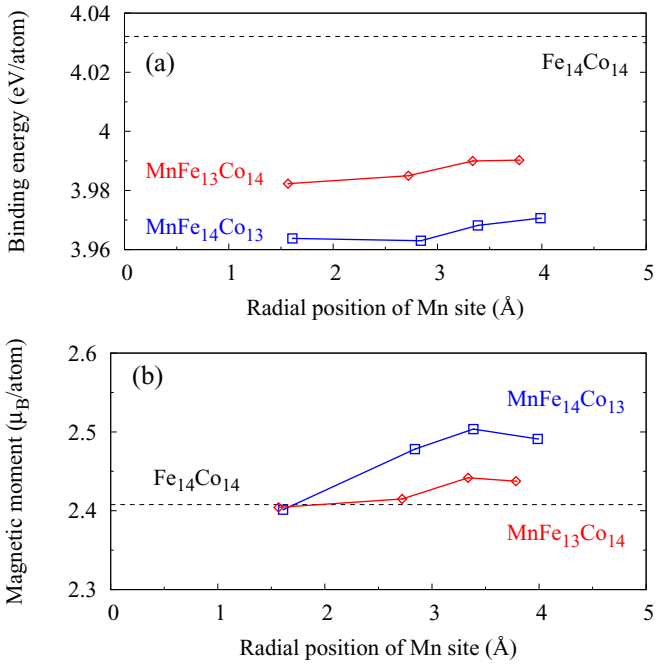

FIG. 2. (a) Binding energies and (b) total magnetic moments of $MnFe_{14}Co_{13}$ and $MnFe_{13}Co_{14}$ clusters as a function of the radial position of substituted Mn atoms. The dotted lines indicate the binding energy and the total magnetic moment of a parent $Fe_{14}Co_{14}$ cluster.

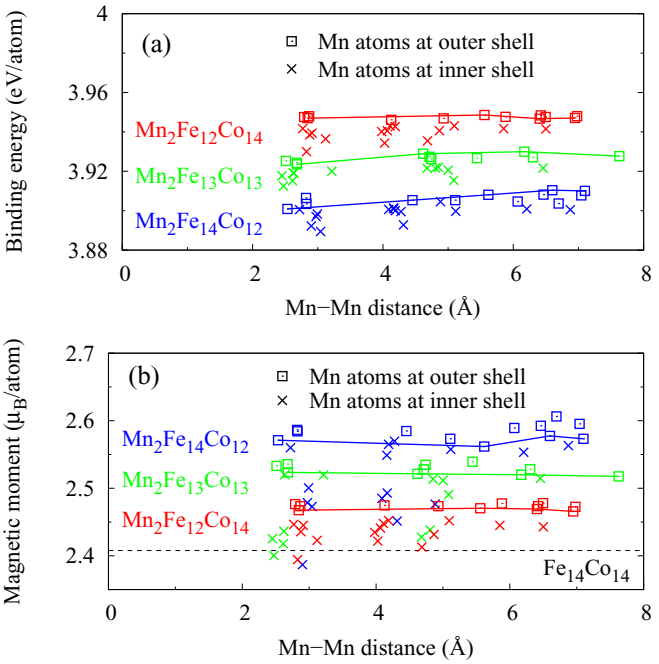

FIG. 3. (a) Binding energies and (b) total magnetic moments of 28-atom $Mn_2Fe_YCo_Z$ clusters with various substitution patterns as a function of the Mn-Mn distance in a cluster. The dotted line in panel (b) indicates the total magnetic moment of the parent $Fe_{14}Co_{14}$ cluster. The solid lines connect the values of MnFeCo clusters with Mn atoms on the outermost shell.

We study 28-atom $Mn_2Fe_YCo_Z$ clusters ($Y + Z + 2 = 28$) to examine the impact of the "second" Mn atom on structural stability and magnetic properties. Figure 3 shows the binding energies and total magnetic moment of $Mn_2Fe_YCo_Z$ clusters with various Mn substitution patterns. The obtained results are practically independent of the Mn-Mn distance because the Mn-Mn distance in a cluster is much longer than that in bulk. Overall, clusters are more stable when two Mn atoms are placed on a cluster surface (outer "shell") and away from each other. As in the case of $MnFe_YCo_Z$ clusters, Fe is more likely to be substituted than Co. Also, substituted Mn atoms prefer ferromagnetic coupling to neighboring Fe and Co atoms. Replacing Co with Mn brings about a larger increase in the total magnetic moment compared with substituting Fe with Mn.

Figure 4 shows the binding energies and total magnetic moments of 28-atom $Mn_XFe_YCo_Z$ clusters with different numbers of Mn atoms. We examined dozens of configurations to find a stable isomer. Three low-energy $Mn_XFe_YCo_Z$ clusters were used as parent structures and one Fe (Co) atom out of Y Fe atoms (Z Co atoms) was randomly substituted with a Mn atom, producing offspring clusters of $Mn_{X+1}Fe_{Y-1}Co_Z$ (or $Mn_{X+1}Fe_YCo_{Z-1}$) with various Mn-doping patterns. For each composition, we extracted three to five low-energy clusters through the structural optimizations. We find that substituted Mn atoms tend to occupy surface sites away from each other, lowering the total energy. The calculated binding energy decreases linearly with the number of Mn atoms, whereas the total magnetic moment increases constantly. The slopes are well related to substitution patterns. In particular, substitution of Mn for Fe (Co) gives a slope of 0.9 (2.4) μ_B per Mn atom. These results agree qualitatively with the experimental and theoretical results on binary MnFe and MnCo clusters [14,16].

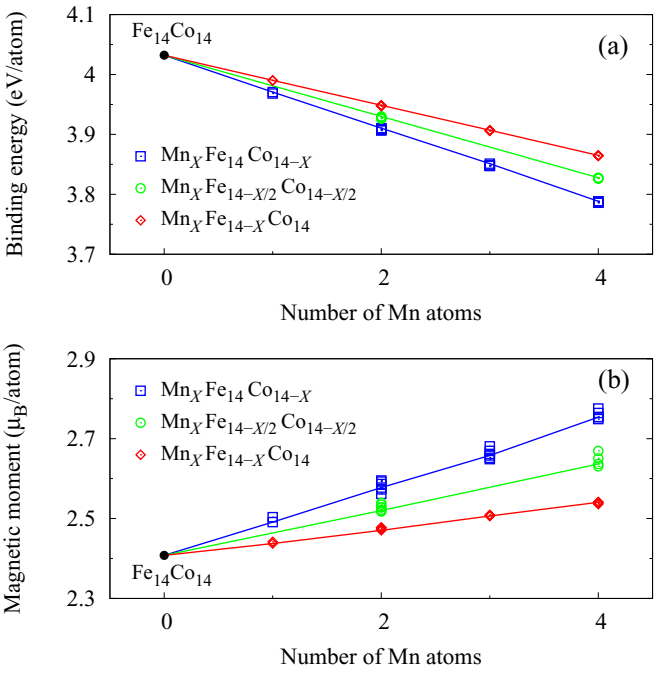

FIG. 4. (a) Binding energies and (b) total magnetic moments for 28-atom $Mn_XFe_YCo_Z$ clusters as a function of the number of Mn atoms (X). The solid lines connect the values of stable isomers.

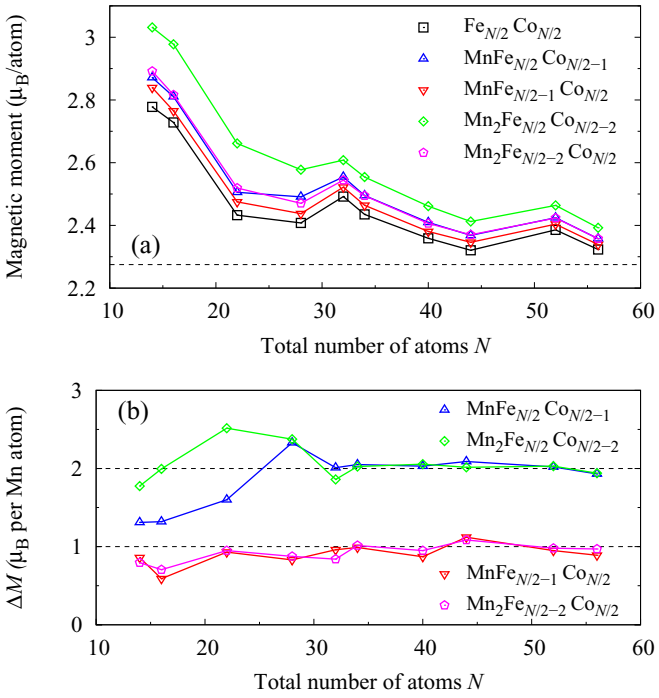

FIG. 5. (a) Size dependence of the total magnetic moments for FeCo and MnFeCo clusters. The dotted line indicates the total magnetic moment of bulk FeCo. (b) Increase of the total magnetic moment per Mn atom after Mn substitution.

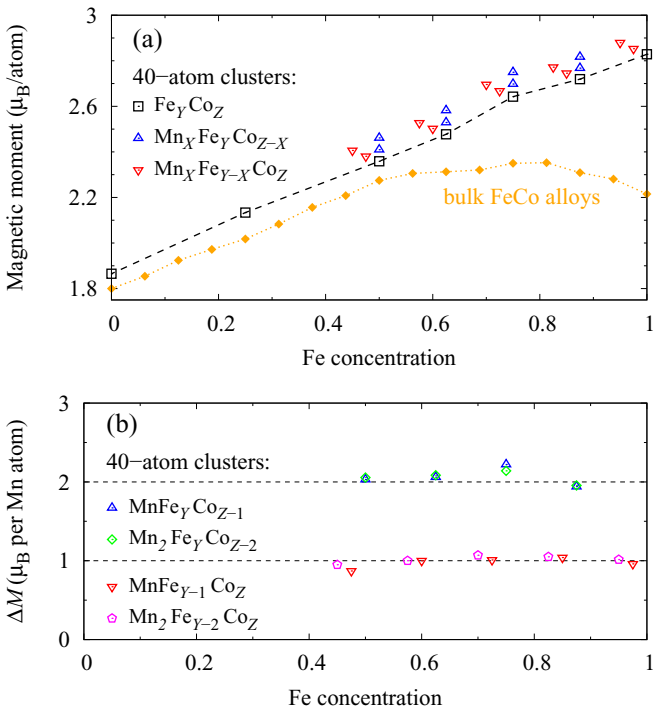

FIG. 6. (a) The total magnetic moments of 40-atom clusters of Fe_YCo_Z, $Mn_XFe_{Y-X}Co_Z$, and $Mn_XFe_YCo_{Z-X}$ ($Y+Z=40$, $X=1,2$), and bulk FeCo alloys with various Fe concentrations. (b) Increase of the total magnetic moment per Mn atom after Mn substitution.

B. Size dependence

We study the size dependence of the magnetic properties of MnFeCo clusters. Figure 5(a) shows the evolution of the total magnetic moments for cluster sizes N of up to 56 atoms. The magnetic moments generally decrease as cluster size increases, with local maxima at $N=32$ and 52. This nonmonotonic behavior of the magnetic moments is similar to those experimentally observed and theoretically analyzed for elemental clusters of Fe, Co, and Ni [1,26–28].

In Fig. 5(b), we plot the difference in the total magnetic moment between FeCo and MnFeCo clusters, which is given by

$$\Delta M = \{M(\mathrm{Mn}_X\mathrm{Fe}_{Y-X}\mathrm{Co}_Z) - M(\mathrm{Fe}_Y\mathrm{Co}_Z)\}/X \qquad (1)$$

for Fe-substituted cases and

$$\Delta M = \{M(\mathrm{Mn}_X\mathrm{Fe}_Y\mathrm{Co}_{Z-X}) - M(\mathrm{Fe}_Y\mathrm{Co}_Z)\}/X \qquad (2)$$

for Co-substituted cases. Here, M is the total magnetic moment of an N-atom cluster ($N=Y+Z$). We find that, except for small clusters, magnetic enhancement is practically constant for clusters with more than 30 atoms. Our DFT-GGA calculations give $\Delta M = 1\mu_B$ ($2\mu_B$) per Mn atom for $\mathrm{Mn}_X\mathrm{Fe}_{Y-X}\mathrm{Co}_Z$ ($\mathrm{Mn}_X\mathrm{Fe}_Y\mathrm{Co}_{Z-X}$) clusters. This magnetic enhancement originates from the difference in the number of valence electrons. Mn has seven electrons in the $3d$ and $4s$ levels, Fe has eight, and Co has nine. Occupations for the spin-up (majority) levels are almost the same for the three elements, and the rest of the electrons fills the spin-down (minority) levels. This results in the imbalance between spin-up and spin-down occupations of $\sim 3.9\mu_B$ for Mn, $\sim 2.9\mu_B$ for Fe, and $\sim 1.9\mu_B$ for Co at the surface of a cluster. The difference in these numbers accounts for the constant magnetic enhancement ΔM found in Mn-doped FeCo clusters. The calculated magnetic moments and their dependencies on Mn concentration can be verified by Stern–Gerlach deflection experiments combined with mass spectroscopy.

C. Fe-rich clusters

We demonstrate that the Mn-induced magnetic enhancement can be possible in MnFeCo clusters with various compositions (Fe-Co concentrations). Here, we focus on Fe-rich 40-atom clusters, as we find in the previous section that the size dependence is rather weak for MnFeCo clusters with more than 30 atoms. The calculated total magnetic moments are plotted as a function of Fe concentration in Fig. 6(a), where we also show the magnetic moments of bulk $\mathrm{Fe}_n\mathrm{Co}_m$ alloys [41] ($n+m=1$) for comparison. Bulk FeCo alloys show a Slater–Pauling magnetization behavior [12,13] and there is a maximum in the magnetic moment curve around the Fe concentration of 0.75. In contrast, the magnetic moments of 40-atom FeCo clusters grow steadily as Fe concentration increases and the moments are larger than those of bulk alloys in a whole range of Fe concentration. It is evident from Fig. 6(a) that substitution of Fe or Co by Mn brings an enhancement in the total magnetic moment. Moreover, its increase per Mn dopant, ΔM, depends very weakly on the Fe concentration, as shown in Fig. 6(b). We obtain $\Delta M = 1\mu_B$ ($2\mu_B$) per Mn atom for $\mathrm{Mn}_X\mathrm{Fe}_{Y-X}\mathrm{Co}_Z$ ($\mathrm{Mn}_X\mathrm{Fe}_Y\mathrm{Co}_{Z-X}$) clusters. As discussed in the previous section, the amount of

the increase of the magnetic moment is accounted for by the difference of the valence electrons in the three elements.

In experiment, it can be difficult to control the stoichiometry of alloy clusters. We have clarified that the surface-Mn-induced magnetic enhancement is robust in ternary MnFeCo clusters with various chemical compositions. This indicates that Mn doping is a simple and easy pathway for synthesizing new nanoparticles with a large magnetic moment.

IV. SUMMARY

We have performed first-principles real-space pseudopotential calculations to investigate the magnetic properties of Mn-doped FeCo clusters. We have shown that Mn is likely to be substituted on a cluster surface. Surface Mn prefers ferromagnetic coupling to neighboring Fe and Co atoms and brings a larger local moment than Fe and Co, resulting in an increase of the total magnetic moment. Magnetic enhancement is found to be robust in ternary MnFeCo clusters with various sizes and different compositions. We anticipate that Mn substitution is a useful guide to design new nanoparticles with a large magnetic moment.

ACKNOWLEDGMENTS

The authors would like to thank C.-Z. Wang (Ames Laboratory) and X. Xu (University of Nebraska–Lincoln) for helpful discussions. M.S. and J.R.C. acknowledge support from a grant from the National Science Foundation (NSF), DMREF-1729202. HPC resources were provided by the Texas Advanced Computing Center (TACC), through XSEDE allocation MCA08X029, and the National Energy Research Scientific Computing Center (NERSC).

[1] I. M. Billas, A. Châtelain, and W. A. de Heer, Science **265**, 1682 (1994).
[2] A. J. Cox, J. G. Louderback, and L. A. Bloomfield, Phys. Rev. Lett. **71**, 923 (1993).
[3] R. Skomski, J. Phys.: Condens. Matter **15**, R841 (2003).
[4] G. B. Haxel, J. B. Hedrick, and G. J. Orris, U.S. Geological Survey, Fact Sheet 087-02 (2002), https://pubs.usgs.gov/fs/2002/fs087-02.
[5] J. M. D. Coey, Scr. Mater. **67**, 524 (2012).
[6] R. J. Snow, H. Bhatkar, A. T. N'Diaye, E. Arenholz, and Y. U. Idzerda, Appl. Phys. Lett. **112**, 072403 (2018).
[7] T. Yamada, N. Kunitomi, Y. Nakai, D. E. Cox, and G. Shirane, J. Phys. Soc. Jpn. **28**, 615 (1970).
[8] D. Hobbs, J. Hafner, and D. Spišák, Phys. Rev. B **68**, 014407 (2003).
[9] H. Yamauchi, H. Watanabe, Y. Suzuki, and H. Saito, J. Phys. Soc. Jpn. **36**, 971 (1974).
[10] D. J. M. King, S. C. Middleburgh, P. A. Burr, T. M. Whiting, P. C. Fossati, and M. R. Wenman, Phys. Rev. B **98**, 024418 (2018).
[11] J. Crangle, Philos. Mag. **2**, 659 (1957).
[12] J. C. Slater, J. Appl. Phys. **8**, 385 (1937).
[13] L. Pauling, Phys. Rev. **54**, 899 (1938).
[14] S. Yin, R. Moro, X. Xu, and W. A. de Heer, Phys. Rev. Lett. **98**, 113401 (2007).
[15] S. Ganguly, M. Kabir, S. Datta, B. Sanyal, and A. Mookerjee, Phys. Rev. B **78**, 014402 (2008).
[16] G. Rollmann, S. Sahoo, A. Hucht, and P. Entel, Phys. Rev. B **78**, 134404 (2008).
[17] M. Pereiro, D. Baldomir, and J. E. Arias, Phys. Rev. B **80**, 075412 (2009).
[18] A. Kashyap, R. Pathak, D. J. Sellmyer, and R. Skomski, IEEE Trans. Magn. **54**, 1 (2018).
[19] B. Das, B. Balasubramanian, P. Manchanda, P. Mukherjee, R. Skomski, G. C. Hadjipanayis, and D. J. Sellmyer, Nano Lett. **16**, 1132 (2016).
[20] J. Friedel, Nuovo Cimento **7**, 287 (1958).
[21] J. R. Chelikowsky, N. Troullier, and Y. Saad, Phys. Rev. Lett. **72**, 1240 (1994).
[22] J. R. Chelikowsky, N. Troullier, K. Wu, and Y. Saad, Phys. Rev. B **50**, 11355 (1994).
[23] L. Kronik, A. Makmal, M. L. Tiago, M. M. G. Alemany, M. Jain, X. Huang, Y. Saad, and J. R. Chelikowsky, Phys. Status Solidi B **243**, 1063 (2006).
[24] P. Hohenberg and W. Kohn, Phys. Rev. **136**, B864 (1964).
[25] W. Kohn and L. J. Sham, Phys. Rev. **140**, A1133 (1965).
[26] M. L. Tiago, Y. Zhou, M. M. G. Alemany, Y. Saad, and J. R. Chelikowsky, Phys. Rev. Lett. **97**, 147201 (2006).
[27] J. Souto-Casares, M. Sakurai, and J. R. Chelikowsky, Phys. Rev. B **93**, 174418 (2016).
[28] M. Sakurai, J. Souto-Casares, and J. R. Chelikowsky, Phys. Rev. B **94**, 024437 (2016).
[29] D. Naveh and L. Kronik, Solid State Commun. **149**, 177 (2009).
[30] J. P. Perdew, K. Burke, and M. Ernzerhof, Phys. Rev. Lett. **77**, 3865 (1996).
[31] M. Sakurai and J. R. Chelikowsky, Phys. Rev. Mater. **2**, 084411 (2018).
[32] M. Sakurai, X. Zhao, C.-Z. Wang, K.-M. Ho, and J. R. Chelikowsky, Phys. Rev. Mater. **2**, 024401 (2018).
[33] N. Troullier and J. L. Martins, Phys. Rev. B **43**, 1993 (1991).
[34] S. G. Louie, S. Froyen, and M. L. Cohen, Phys. Rev. B **26**, 1738 (1982).
[35] R. H. Byrd, P. Lu, J. Nocedal, and C. Zhu, SIAM J. Sci. Comput. **16**, 1190 (1995).
[36] C. Zhu, R. H. Byrd, P. Lu, and J. Nocedal, ACM Trans. Math. Software **23**, 550 (1997).
[37] J. L. Morales and J. Nocedal, ACM Trans. Math. Software **38**, 1 (2011).
[38] Y. Zhou, Y. Saad, M. L. Tiago, and J. R. Chelikowsky, Phys. Rev. E **74**, 066704 (2006).
[39] Y. Zhou, Y. Saad, M. L. Tiago, and J. R. Chelikowsky, J. Comput. Phys. **219**, 172 (2006).
[40] Y. Zhou, J. R. Chelikowsky, and Y. Saad, J. Comput. Phys. **274**, 770 (2014).
[41] A. Díaz-Ortiz, R. Drautz, M. Fähnle, H. Dosch, and J. M. Sanchez, Phys. Rev. B **73**, 224208 (2006).